Proceedings World Geothermal Congress 2023
Beijing, China, October 9 – 11, 2023

Numerical Modeling of Permeability Enhancement and Induced Seismicity during EGS Operation using a Partially Bridging Multi-Stage Hydraulic Fracture design

Pengliang Yu[1,4], David Dempsey[2], Rosalind Archer[3], Chris Marone[4], Derek Elsworth[4]

[1] Geothermal Institute, Department of Engineering Science, University of Auckland, Auckland, New Zealand

[2] Department of Civil and Natural Resources Engineering, University of Canterbury, Christchurch, New Zealand

[3] School of Engineering and Built Environment, Griffith University, Queensland, Australia

[4] EMS Energy Institute, Departments of Geosciences and of Energy and Mineral Engineering, The Pennsylvania State University, University Park, PA 16802, USA

Email address: pyu340@aucklanduni.ac.nz; pmy5077@psu.edu

Keywords: Enhanced geothermal system, partially bridging multi-stage fractures, horizontal wells, thermal-hydraulic-mechanical, permeability enhancement, induced-seismicity

ABSTRACT

Enhanced geothermal systems (EGS) have emerged as an alternative energy supply that is both green and tackles climate change. Multi-stage hydraulic fractured horizontal well design is a promising design for economic EGS development. In our previous work, we proposed a partially bridging fracture pattern that forces water to flow through the stimulated reservoir volume (SRV) of an EGS, which improves heat extraction efficiency. In this work, we use a fully coupled thermal-hydraulic-mechanical (THM) model, developed in the reservoir simulator, FEHM, to evaluate the associated induced seismicity and secondary permeability enhancement in the SRV during production for the proposed EGS design. The model includes coupled reservoir and horizontal wellbore components that account for the thermo-poroelastic induced stress changes and permeability enhancement over a 20-year production period. A Mohr-Coulomb failure criterion and empirical fracture permeability model are applied to describe permeability evolution and induced microseismicity associated with the stress evolution in the system. We use these to evaluate the style of permeability enhancement, and the rate of triggered seismic events. We found that SRV permeability may be significantly enhanced during 20 years of production, leading to a higher total amount of thermal energy extraction, higher rates of induced seismicity but earlier thermal breakthrough.

1. INTRODUCTION

The heat energy stored in impermeable hot dry rock (HDR) at depths of 2 - 10 km and thus at temperatures between 150 and 650℃ is an enormous potential resource for both generating electricity and for direct use (Tester et al., 2006; Chamorro et al., 2014; Lei et al., 2020). Enhanced geothermal systems (EGS) have been proposed to accelerate the production of thermal energy from HDR via the application of stimulation technologies including hydraulic fracturing, hydroshearing, thermal stimulation or chemical stimulation. These interventions improve permeability and potentially fluid-rock contact area for heat transfer (Dempsey et al. 2015; Norbeck et al., 2018; Moore et al., 2019).

In recent years, the application of horizontal well drilling and multi-stage hydraulic fracturing technologies have been investigated, from theoretical and practical perspectives, to create artificial fracture networks with large stimulated reservoir volumes (SRV) (Shiozawa & McClure, 2014; Jung, 2013; Xu et al., 2018; Han et al., 2019). Our previous research (Yu et al., 2021) proposed a multi-stage partially bridging fracture doublet horizontal well EGS design to force the flow of water through the SRV. This design is a modification of the fully bridging fracture design proposed by Gringarten et al. (1975), as shown in Fig.1. In the fully bridging fracture design (Fig.1a), cold water flows directly from the injection well to production well *via* connected hydraulic fractures. In this case, the size of the heat extraction zone is limited by the penetration length of injected water into the SRV.

The partially bridging fracture design could increase mass flow rates of water through the SRV (Fig.1b). Half of the hydraulic fractures are propagated from the production well but are stopped short of the injection well. The other half are grown from the injection well and stop short of the production well. Therefore, hydraulic fractures in the partially bridging fracture design do not directly connect the injection and production wells. This novel design would force the water injected from injection well to enter and flow through the SRV, later exiting in the fractures connected to the production well.

In our previous work, we built thermo-hydraulic-mechanical (THM) coupling numerical models to compare the thermal performance between partially and fully bridging fracture design. This indicated that the partially bridging design (Fig.1b) could produce water with higher temperature for the same total volume of circulated water, suggesting an improved heat sweep and delayed short-circuiting. We also analyzed the techno-economic feasibility of the proposed design for direct heating applications, quantifying economic and environmental benefits (Yu et al., 2022).

Although our theoretical results demonstrated that partially bridging fractures would promote extensive secondary shear failure due to thermo-poroelastic stressing, the associated permeability enhancement was not evaluated. However, such enhancement over the production period, particularly within the SRV, can be expected to affect thermal performance and breakthrough. In addition, there is also a need to consider induced microseismicity, and whether this is exacerbated for particular fracture designs or by secondary stimulation processes.

In this study, we developed a 3D THM coupled numerical model in an engineered reservoir with a wellbore system that uses a multi-stage partially bridging fracture doublet horizontal well EGS design. We use the stress-dependent permeability simulation framework developed by Dempsey et al. (2015) to evaluate this sub-grid-scale permeability enhancement during the production period. The thermal performance and permeability evolution during the operational period is analyzed for the proposed partially bridging fracture EGS design. In addition, we modelled induced seismicity over the production period as a function of the volume-weighted excess shear stress change (Riffault, 2019). The spatiotemporal evolution of seismicity rate is investigated.

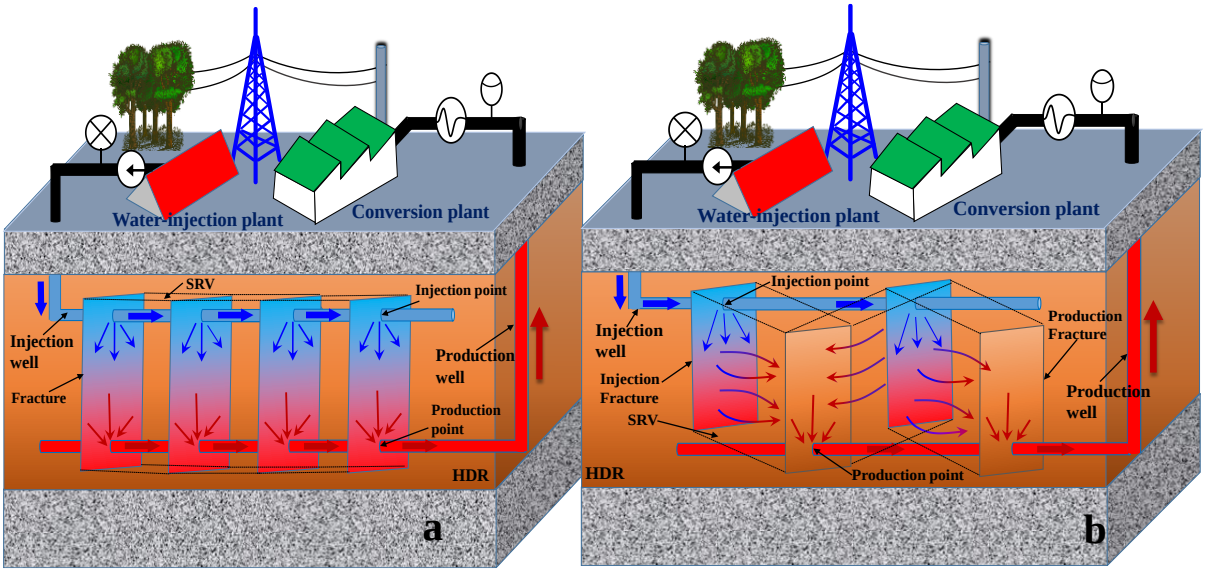

Figure1: Schematic diagram of EGS designs with paired horizontal injection and production wells, and two fracture designs connecting them. (a) Fully-bridging hydraulic fractures, after Gringarten (1975) (b) Partially-bridging hydraulic fractures, after Yu et al. (2021). Arrows denote fluid flow pathways.

2. THM COUPLING AND PERMEABILITY ENHANCEMENT NUMERICAL MODEL CONSTRUCTION

We established the 3D THM coupling numerical model for the proposed multiple partially bridging fracture doublet horizontal well EGS design using the Finite Element Heat and Mass transfer (FEHM) simulator (Zyvoloski et al., 1997). In this numerical model, we construct both reservoir and horizontal wellbore compartments to capture the heat, mass flow and rock mechanics characteristics, which reflect the mixing processes in long horizontal wellbores with multiple perforations allowing fluids to enter from, and exit into, the reservoir. The governing equations for mass, energy and stress balance used in the FEHM are (Kelkar et al., 2014):

$$\frac{\partial}{\partial t}(\rho_w \varphi) + \nabla \cdot \boldsymbol{q} = Q_m \tag{1}$$

$$\boldsymbol{q} = -\frac{\rho_w k}{\mu}(\nabla p + \rho_w \boldsymbol{g}) \tag{2}$$

$$\left(\rho c_p\right)_{eff} \frac{\partial T}{\partial t} + \nabla \cdot \left(c_{p,w} \boldsymbol{q} T\right) - \nabla \cdot (\lambda_m \nabla T) = Q_E \tag{3}$$

$$\nabla \boldsymbol{\sigma} + \rho_r \boldsymbol{b} = 0 \tag{4}$$

$$\boldsymbol{\sigma} = \lambda tr(\boldsymbol{\epsilon})\boldsymbol{I} + 2G\boldsymbol{\epsilon} + (\beta \Delta p + \alpha E \Delta T)\boldsymbol{I} \tag{5}$$

$$\boldsymbol{\epsilon} = \frac{1}{2}[\nabla \boldsymbol{u} + (\nabla \boldsymbol{u})^T] \tag{6}$$

where ρ_w, μ, $c_{p,w}$ are the density, viscosity, specific heat capacity of the fluid; φ, k, ρ_r are porosity, permeability and density of the rock. $\left(\rho c_p\right)_{eff}$ and λ_m are effective volumetric heat capacity and thermal conductivity, $\boldsymbol{\sigma}$ and $\boldsymbol{b}$ are the stress tensor and body force vector, $\boldsymbol{\epsilon}$ and $\boldsymbol{u}$ are the strain tensor and displacement vector, λ, G ,E, α and β are Lamé's parameter, shear modulus, Young's modulus, coefficient of thermal expansion and the Biot coefficient, $\boldsymbol{g}$ is gravity, p and T are pressure and temperature, and Q_m and Q_E are mass and energy source terms. In the simulation model, permeability is calculated as a function of $\boldsymbol{\sigma}$ (Section 2.2), which is then updated at the end of each time step.

2.1 EGS reservoir and horizontal wellbore models

The computational domain built in this study is subdivided into an unstimulated reservoir zone enclosing separate SRVs and fracture zones, as well as horizontal injection and production well zones. In this study, we used a design that comprises four idealized and partially bridging fractures and three intervening SRV zones. The computational domain spans a 2000×500×300 m volume centered at a depth of 3000 m. Vertical fractures are evenly distributed between the toe and heel of the wellbore (Fig.2a). The fracture height

and aperture are 30m and 1mm respectively. The fracture length is 300m but could be altered to analyze the effect of fracture length on thermal performance.

In the horizontal wellbore model, we considered the flow inside of wellbore boundary and the associated perforations on the horizontal wellbores that provide flow linkages between fractures and wells. The wellbore model is built in FEHM by assignment of node properties (Fig.2b) to represent the horizontal wellbores, casing, and fracture perforations located along the wellbore boundary (Dempsey et al., 2015; Yu et al., 2022). Well nodes are assigned 100% porosity and high permeability, while the casing is impermeable and has zero porosity. Perforation nodes are assigned the same permeability and porosity as the fractures. As shown in Fig.2b, Water is injected into the injection wellhead node where it flows along the wellbore and through the injection perforation nodes into the injection fractures. From there, it flows across the SRV zones to advect the heat delivered from the rock matrix. Water exits into the production fractures and from there into the horizontal production wellbore *via* the production perforation nodes, exiting at the production wellhead node. Representative parameters for reservoir and wellbore simulators are listed in Table 1. For detailed introduction, please refer to Yu et al. (2022).

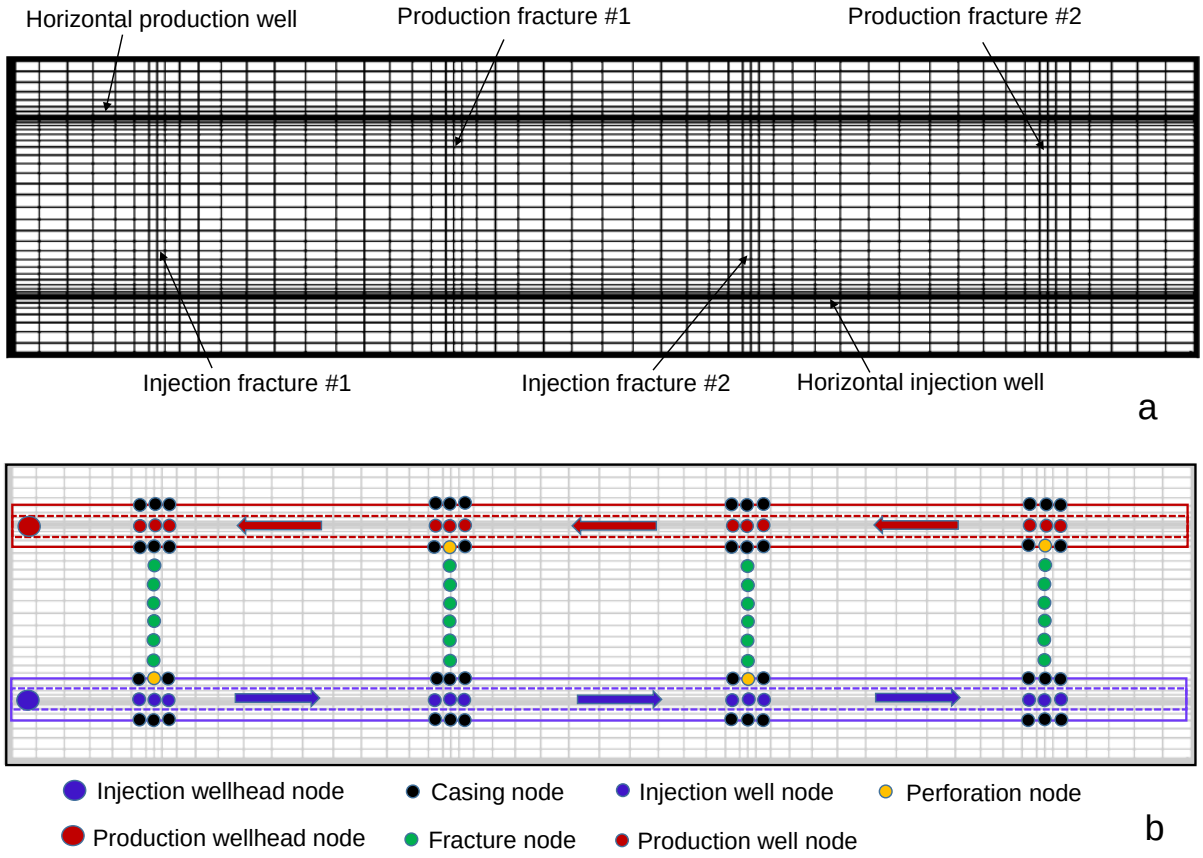

Figure 2: (a) Vertical section through reservoir (x-y plane view) of model mesh for four partially bridging fracture models and (b) a schematic diagram of node assignments and connections in the FEHM framework. Mesh spacings are indicative only.

Table 1: Physical parameters of reservoir-fracture-well model (Dempsey et al. 2015; Yu et al., 2022).

Parameters	Background rock	SRV	Fracture & perforations	Wellbore	Casing
Density (kg/m^3)	2500	2500	-	-	2500
Heat conductivity (W/(m·K))	2.5	2.5	-	-	2.5
Heat capacity (J/(kg·K))	1000	1000	-	-	1000
Porosity (%)	1	2	100	100	0
Permeability (m^2)	10^{-16}	5×10^{-15}	6.2×10^{-12}	5×10^{-9}	10^{-18}

Young's modulus (GPa)	60	60	-	-	60
Poisson's ratio	0.2	0.2	-	-	0.2
Thermal expansion coefficient (K^{-1})	5×10^{-6}	5×10^{-6}	-	-	5×10^{-6}
Biot coefficient	0.5	0.5	-	-	0.5

2.2 Stress-dependent permeability model

In order to simulate reservoir permeability enhancement during 20 years of production and rock cooling, we used the stress-dependent permeability model developed by Dempsey et al. (2015). In this model, each reservoir control volume (computational node) in the FEHM model includes a number of throughgoing, non-intersecting, variably oriented fractures that do not interact mechanically. Each of these fractures has some initial permeability that can change according to the local stresses and Mohr-Coulomb failure criterion.

Failure of each fracture is assessed in terms of the Mohr-Coulomb criterion, which is here formulated in terms of the excess shear stress, τ_{ex}, describing the proximity to failure:

$$\tau_{ex} = |\tau| - \mu_s(\sigma_n - p) - S_0 \tag{7}$$

where τ and σ_n are the shear and normal stress on the fracture, p is the fluid pressure in the fracture, and μ_s and S_0 are the static coefficient of friction and cohesion. Excess shear stress is generally less than zero for stable fractures, which indicates the current shear stress on the fracture is too small to overcome the combined stabilizing influence of static friction and cohesion. As τ_{ex} approaches zero, the fracture becomes critically stressed; when it reaches zero, the fracture fails. Eq.(7) considers two of the mechanisms contributing to this failure; (i) an increase in fluid pressure within the fracture; and (ii) a decrease in the normal stress due to cooling.

The nodal permeability is calculated as the ensemble sum of all fracture permeabilities within the control volume of that node. An empirical equation is used to describe the relationship between shear displacement, u,and permeability enhancement, Δk (Lee et al., 2002; Dempsey et al., 2015):

$$\Delta k = \frac{\Delta k_{max}}{1+\exp\left(\ln(19)\times\left(1-2\frac{u-u_5}{u_{95}-u_5}\right)\right)} \tag{8}$$

where Δk_{max} is the maximum change in permeability, and u_5 and u_{95} are the shear displacement at which Δk is 5% and 95% of the maximum. Because Δk is an absolute change in logarithm-space, it corresponds to a multiplier of the untransformed permeability, i.e., $k' = 10^{\Delta k} \times k$. In this paper, we have used the values from Dempsey et al. (2015), who developed a history-matched model for EGS shear stimulation at the Desert Peak geothermal system in Nevada: Δk_{max}=1.7 log (m^2), u_5=$1 \times 10^{-3} m$, u_{95}=$7 \times 10^{-3} m$, initial SRV permeability k=$5 \times 10^{-15} m^2$, fractures per control volume, $N = 100$, shear fracture stiffness, $K_s = 5 \times 10^2 \mathrm{MPa}/m$, dynamic friction coefficient, $\mu_d = 0.65$, $S_0 = 0$, $\mu_s = 0.75$.

The permeability enhancement and SRV permeability change under different shear displacements is shown in Fig.3; the SRV permeability increases from an initial permeability of $5 \times 10^{-15} m^2$ with an increase in shear displacement. The maximum SRV permeability resulting from shear-slip within the reservoir is $2.5 \times 10^{-13} m^2$. The reservoir permeability will maintain its maximum even if the shear displacement continues to increase as shown in the Fig.3b. Although there is significant uncertainty in the parameters used in the model, the qualitative response of a partially bridging fracture-wellbore-reservoir system may be recovered – honoring the principal physical feedbacks in such a system.

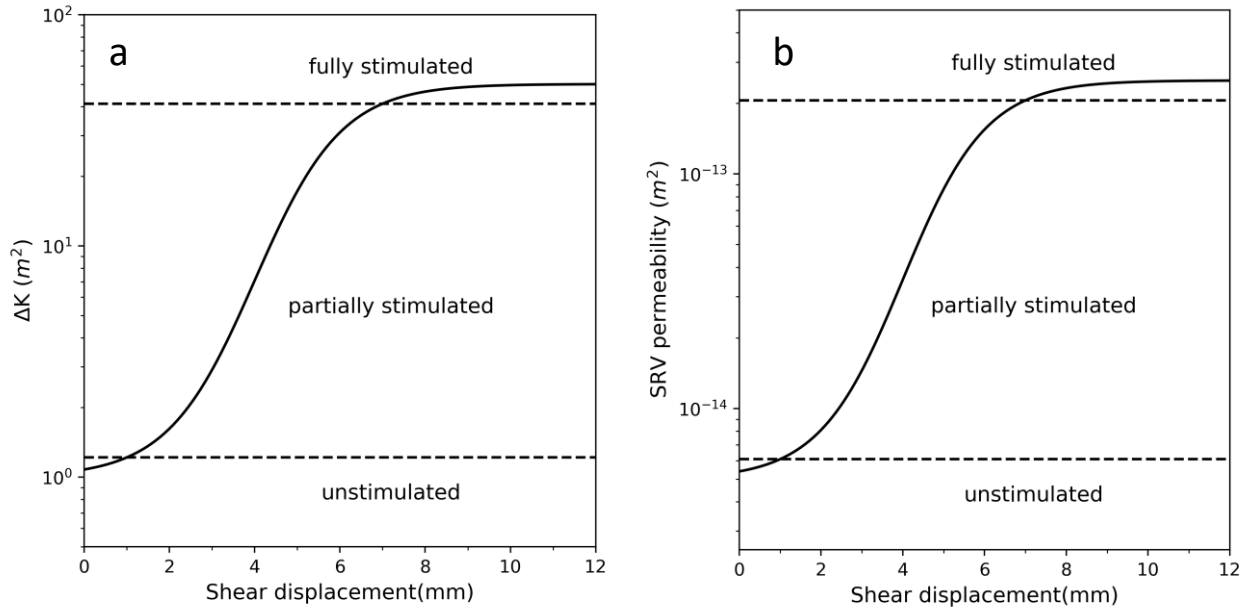

Figure 3: Permeability enhancement (a) SRV permeability (b) model under different shear displacement used in this study based on Eq.(8)

2.3 Induced seismicity rate model

The normal and shear stress depend on the orientation of the fracture relative to the principal stresses and may be expressed as:

$$\sigma_n = \frac{1}{2}(\sigma_1 + \sigma_2) + \frac{1}{2}(\sigma_1 - \sigma_3)\cos(2\theta) \tag{9}$$

$$\tau = \frac{1}{2}(\sigma_1 - \sigma_3)\sin(2\theta) \tag{10}$$

where σ_1,σ_3 are the maximum and minimum principal stresses, and θ is the angle between the fracture plane and orientation of the maximum principal stress. The fracture orientation most likely to fail in shear is $\theta = \frac{\pi}{4} + \arctan(\mu_s)$, which corresponds to:

$$\tan\theta = -\frac{1}{\mu_s} \tag{11}$$

therefore, the excess shear stress may be expressed as:

$$\tau_{ex} = \frac{1}{2}(\sigma_1 - \sigma_3)(\mu_s^2 + 1)^{1/2} - \frac{1}{2}\mu_s(\sigma_1 + \sigma_3) + \mu_s P - S_0. \tag{12}$$

We assume that induced seismicity is a function of the calculated excess shear stress, τ_{ex}, as it originates due to the occurrence of shear slip. Riffault et al. (2018) showed that it is possible for small fractures to fail and generate microseismic events but not necessarily generate an increase in bulk permeability, which depends more on the size of fractures and their interconnectedness. Further, small stress variations are able to trigger shear failure (Townend and Zoback, 2000). Hence, we use the following model for induced earthquakes: events are generated whenever excess shear stress is increased in the computational nodes, and there is no minimum threshold that must be exceeded, contrary to our permeability model. Therefore, as nodes and where time steps with $\Delta\tau_{ex} = \frac{d\tau_{ex}}{dt} > 0$, the total induced seismicity rate, λ, of whole reservoir is expressed as:

$$\lambda = \sum_{n=1}^{n_{tot}} k_s \times \Delta\tau_{ex} \times V_n \tag{13}$$

where k_s is the seismogenic density, $\Delta\tau_{ex}$ is the change in excess shear stress of node n for a given time step t, V_n is the control volume associated with the node n, n_{tot} is the total number of the computational nodes used in the FEHM simulator of the four partially bridging fractures in the model.

2.4 Initial and boundary conditions

The initial reservoir temperature increases linearly from the upper boundary ($z = -2850\ m$) to the lower boundary ($z = -3150m$) of the computational domain with a high assumed geothermal gradient of 0.06 °C/m. The temperature at the upper surface of the reservoir is 250°C. Initial fluid pressure was assumed to be hydrostatic and calculated as $p_i = \rho_w g z$, where z is the reservoir depth and varies between -2850 and -3150 m. We assume an extensional stress regime in the model, the initial vertical stress $\sigma_1 = \sigma_z = \sigma_v = \rho_r g z$, where ρ_r is the density of the reservoir. The initial minimum horizontal principal stress, $\sigma_3 = \sigma_h = \sigma_x$ is determined as $0.61\sigma_z$. The initial maximum horizontal principal stress, $\sigma_2 = \sigma_H = \sigma_y$ is calculated as half of the sum of σ_v and σ_h

(Dempsey et al. 2015). All model boundaries were closed to heat and mass flow. Roller displacement boundary conditions are applied to all boundaries of model.

Fluid with an initial temperature of 30°C was injected at the wellhead node of the injection well with a fixed and constant injection pressure. The constant injection pressure is the maximum pump injection pressure that is equal to the minimum principal stress, which is designed to estimate maximum injection pressure allowed that could avoid propagation of the main hydraulic fractures. The minimum principal stress is calculated assuming a critically stressed crust limited by Mohr-Coulomb frictional failure in a normal faulting environment. Thus, p_{max} is given by (Jaeger et al. 2009):

$$p_{max} = (\sigma_v - p_f)\left(\mu_s + \sqrt{1+\mu_s^2}\right)^{-2} + p_f. \quad (13)$$

A typical value of μ_s = 0.75 is used in this study. For example, at a depth of 2850 m, σ_v = 69.9 MPa, the initial reservoir pressure p_f is 280 MPa, and the constant injection pressure is 38.5 MPa, representing a permissible fluid pressure increase of 10.5 MPa. The pressure in the horizontal production well is also fixed, which is 5 MPa lower than the reservoir initial pressure. This value is sufficiently low to ensure that fluid does not generally flash to steam in the wellbore.

3. SIMULATION RESULTS

In this section, we first compare the thermal performance between models accommodating SRV permeability enhancement and those with fixed SRV permeability. The goal is to evaluate the effect of permeability evolution on both thermal energy extraction and reservoir impedance (injectivity) over 20 years of production (Section 3.1). We also show permeability and temperature contours at different locations and times to analyze the distribution and style of permeability enhancement and resulting breakthrough. Section 3.2 compares the seismicity rate and cumulative seismicity over 20 years. The spatial distribution of seismicity within the reservoir is also investigated.

3.1 Thermal performance of contrasting constant and enhanced SRV permeability models

Models with and without permeability enhancement produce water at different rates and are therefore not directly comparable at the same time. Instead, we compared production temperature and injectivity enhancement as a function of cumulative energy extraction between different models. Injectivity is defined as the ratio of volumetric injection flow rate to injection pressure across the reservoir. Injectivity enhancement is defined as the ratio of injectivity to initial injectivity. As shown in Fig.4, permeability enhancement models accelerate thermal breakthrough (Fig.4a) and increases the injectivity significantly compared to the assumption of static permeability. This is because, as SRV permeability is increased during production, a larger volume of water can be injected into and flow through the SRV domain under the fixed pressure injection-production conditions. This accelerates cooling and leads to an earlier thermal breakthrough.

Although thermal breakthrough is observed earlier when permeability enhancement is taken into account, the extracted total heat energy is approximately double that where no SRV permeability enhancement is accommodated. This also suggests that both the extent and timing of thermal breakthrough, as well as the amount of total extracted heat energy, are underestimated when neglecting secondary stimulation during long-term EGS operation.

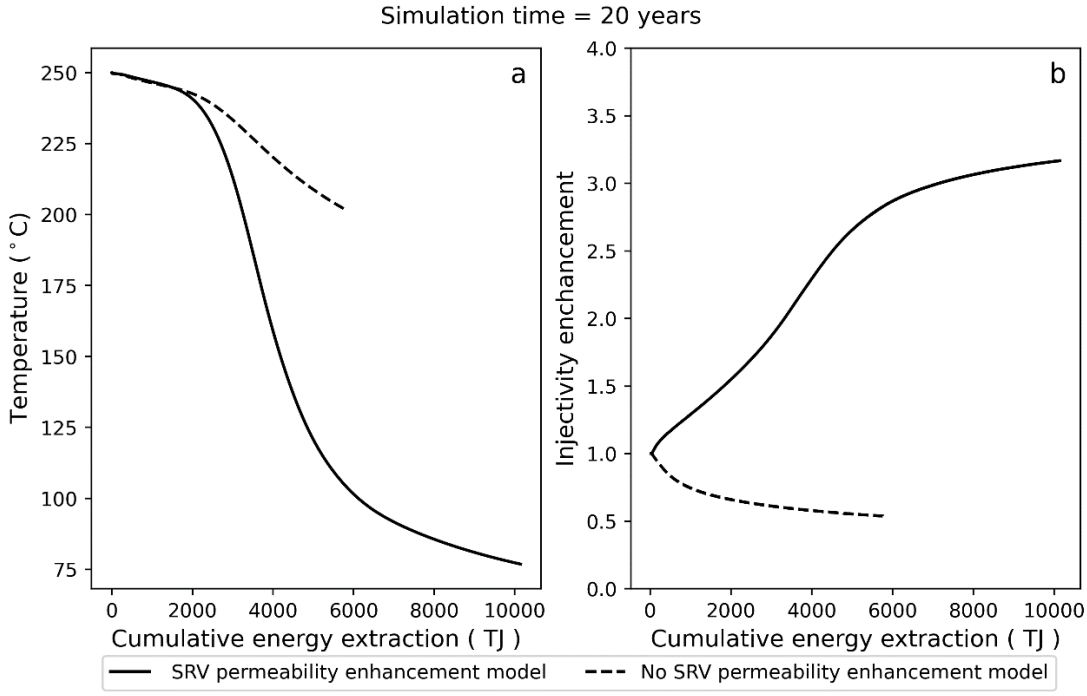

Figure 4: Comparison of (a) temperature and (b) injectivity enhancement between SRV permeability enhancement (solid line) and non-enhancement models (dashed) during a 20 year production period. For a parametrically consistent comparison, model quantities are plotted against cumulative energy extraction rather than time.

We analyzed permeability and temperature distributions when approaching thermal breakthrough (t = 2.5, 4, 5.5 years). Figs. 5-7 show contours through a horizontal(z-) plane at 3000 m, with the thermal front moving from the injection fracture to the production fracture through the SRV. Permeability enhancement fronts follow a similar pattern, moving from the side of the injection fracture to the production fracture. This is because the effective normal stress close to the injection fracture is decreased due to cooling and pressurization, both of which increase the excess shear stress and promote fracture failure. After 5.5 years, most of the SRV has experienced some degree of permeability enhancement, although this result will vary in different parameterizations.

Between 4 and 5.5 years, thermal breakthrough is observed as a sharply decreasing production temperature (Fig.7b), consistent with the permeability enhancement trend. At the same time, there is reasonably close correspondence between distributions of temperature and permeability enhancement. This suggests that if one could be measured, it might be used as a proxy for the other.

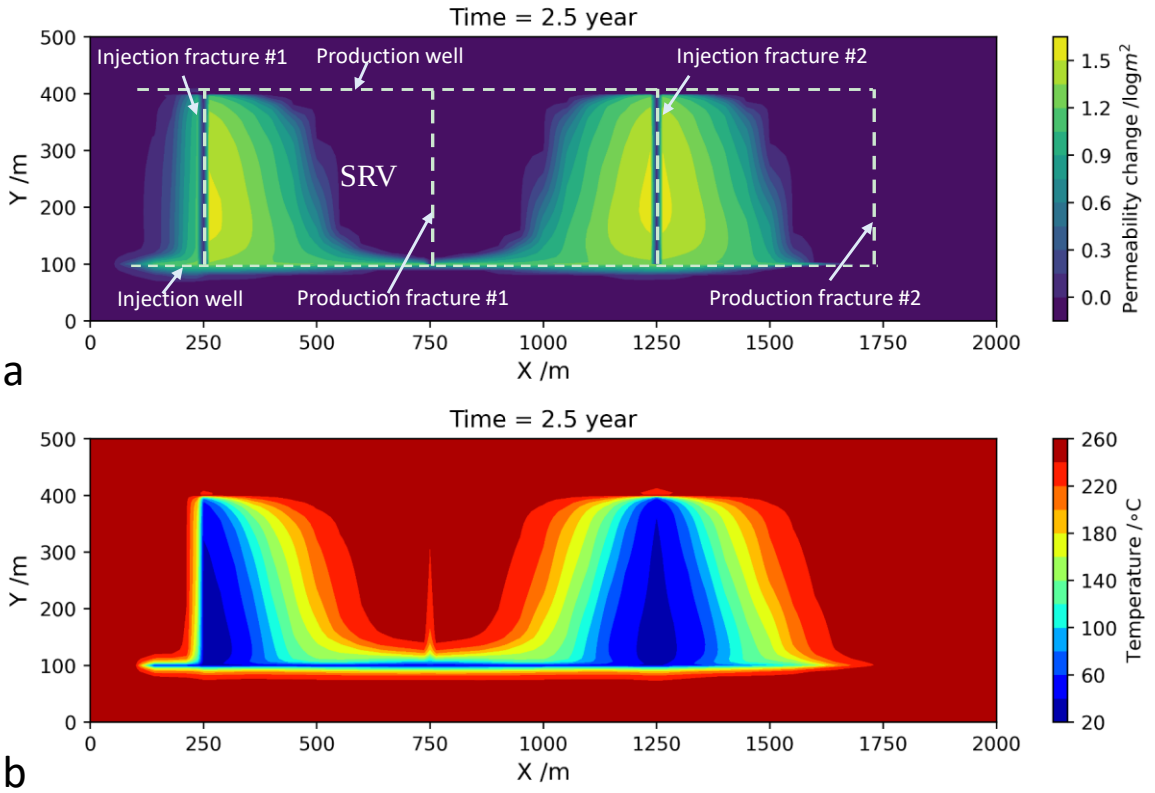

Figure 5: Permeability enhancement (a) and temperature (b) distribution on a horizontal plane cutting the reservoir at a depth of z = -3000m at t = 2.5 years for the SRV permeability enhancement model using four partially bridging fracture doublets linked by horizontal wells penetrating an EGS reservoir. Note: (a) also shows the locations of injection fractures, production fractures, injection and production wells and the SRV as white dotted lines.

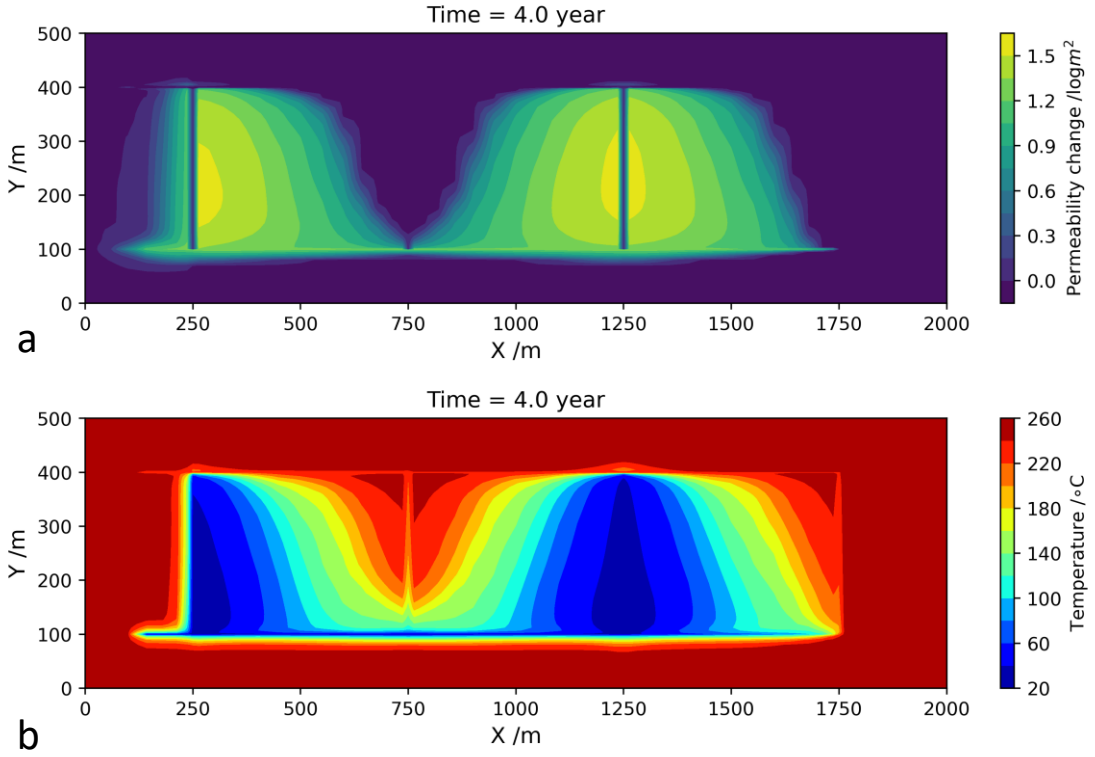

Figure 6: Permeability enhancement (a) and temperature (b) distributions on a horizontal plane cutting the reservoir at a depth of z = -3000m at t = 4 years for the SRV permeability enhancement model using four partially bridging fracture doublets linked by horizontal wells penetrating an EGS reservoir.

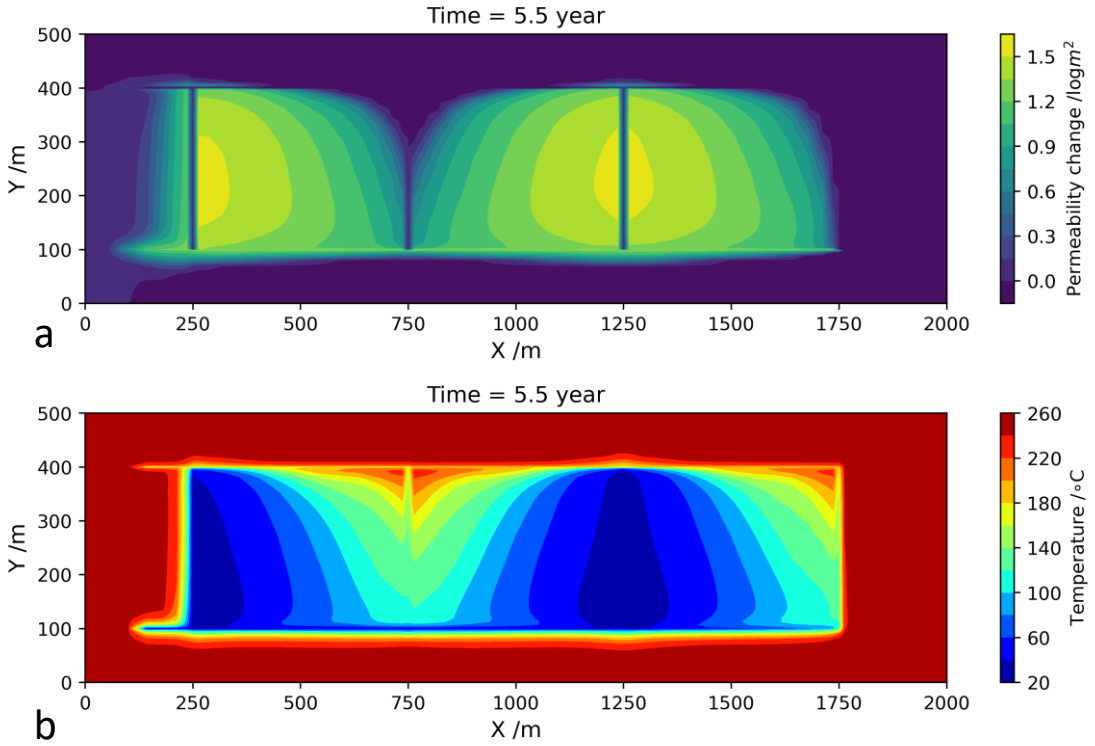

Figure 7: Permeability enhancement (a) and temperature (b) distributions on a horizontal plane cutting the reservoir at a depth of z = -3000m at t = 5.5 years for the SRV permeability enhancement model using four partially bridging fracture doublets linked by horizontal wells penetrating an EGS reservoir.

3.2 Induced seismicity rate of contrasting constant and enhanced SRV permeability models

Fig. 8 shows how the relative seismicity rate changes over time for models with and without permeability enhancement. The relative seismicity rate has been defined as the ratio the current seismicity rate to the average seismicity rate over 20 years for a constant permeability model.

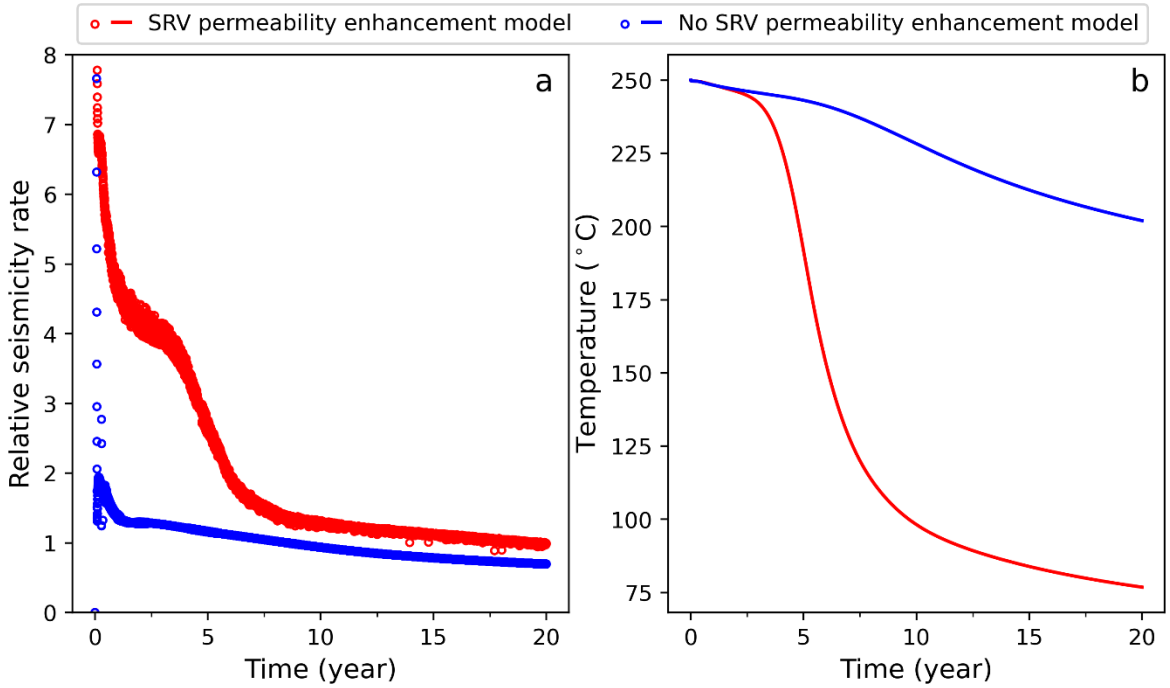

Figure 8: Relative seismicity rate (a) and temperature (b) change over 20 years production comparison between the permeability enhancement ond constant permeability models for the SRV.

As shown in Fig. 8, the seismicity rates decrease over time for models both with and without permeability enhancement. The maximum seismicity rate is observed in the early production period for both models. This might be because the most significant thermal contraction is triggered by cooling water injection (largest temperature gap between injection temperature and reservoir temperature), thereby resulting in extensive excess shear rate changes near the injection fracture area at early production time.

For the model with permeability enhancement, most seismicity is observed before thermal breakthrough (Fig. 8) with the seismicity rate dropping significantly during thermal breakthrough. During this time, the temperature difference and induced thermal stress within the reservoir becomes much smaller.

Fig. 9 shows the relative cumulative seismicity for models both with and without permeability enhancement. The relative cumulative seismicity is defined as the ratio between cumulative seismicity and total seismicity at the end of the 20-year simulation for the reservoir without permeability enhancement. Although more energy is extracted when permeability enhancement accommodated, there are also more induced earthquakes. Interestingly, the permeability enhancement model generates more events per unit of energy extracted from the reservoir. This makes sense because extracting energy involves decreasing rock temperature, which induces larger thermal stresses. Hence, there is a trade-off between maximizing cumulative energy extraction from an EGS while accepting some degree of seismicity.

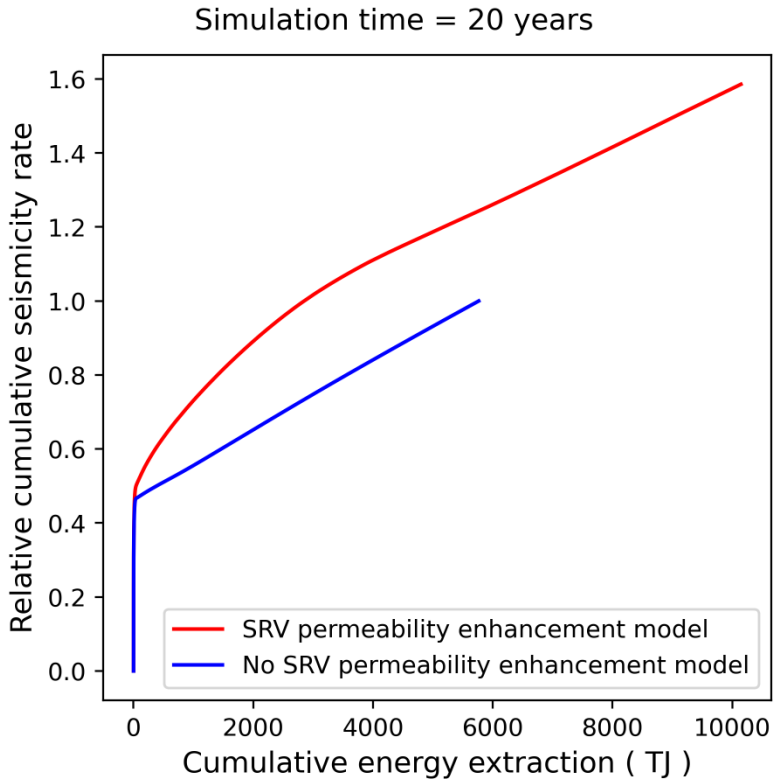

Figure 9: Relative cumulative seismicity rate for models both with and without permeability enhancement.

Fig. 10 shows the evolution of the spatial pattern in seismicity during thermal breakthrough (t = 2.5, 4, 5.5 years) for the model with permeability enhancement. The areas of densest seismicity migrate from the injection fractures towards the production fractures with increased time. Furthermore, the relative seismicity rate is decreases significantly as the contrast between injection temperature and reservoir temperature drops during breakthrough. Comparing the seismicity patterns (Fig.10) to temperature and permeability enhancement evolution (Fig.5-7), it may later be possible to use seismicity as a constraint on cooling and secondary stimulation during EGS production. This idea has been applied in EGS stimulation by Riffault (2019), who used short-term seismicity data to map the permeability distribution after stimulation tests.

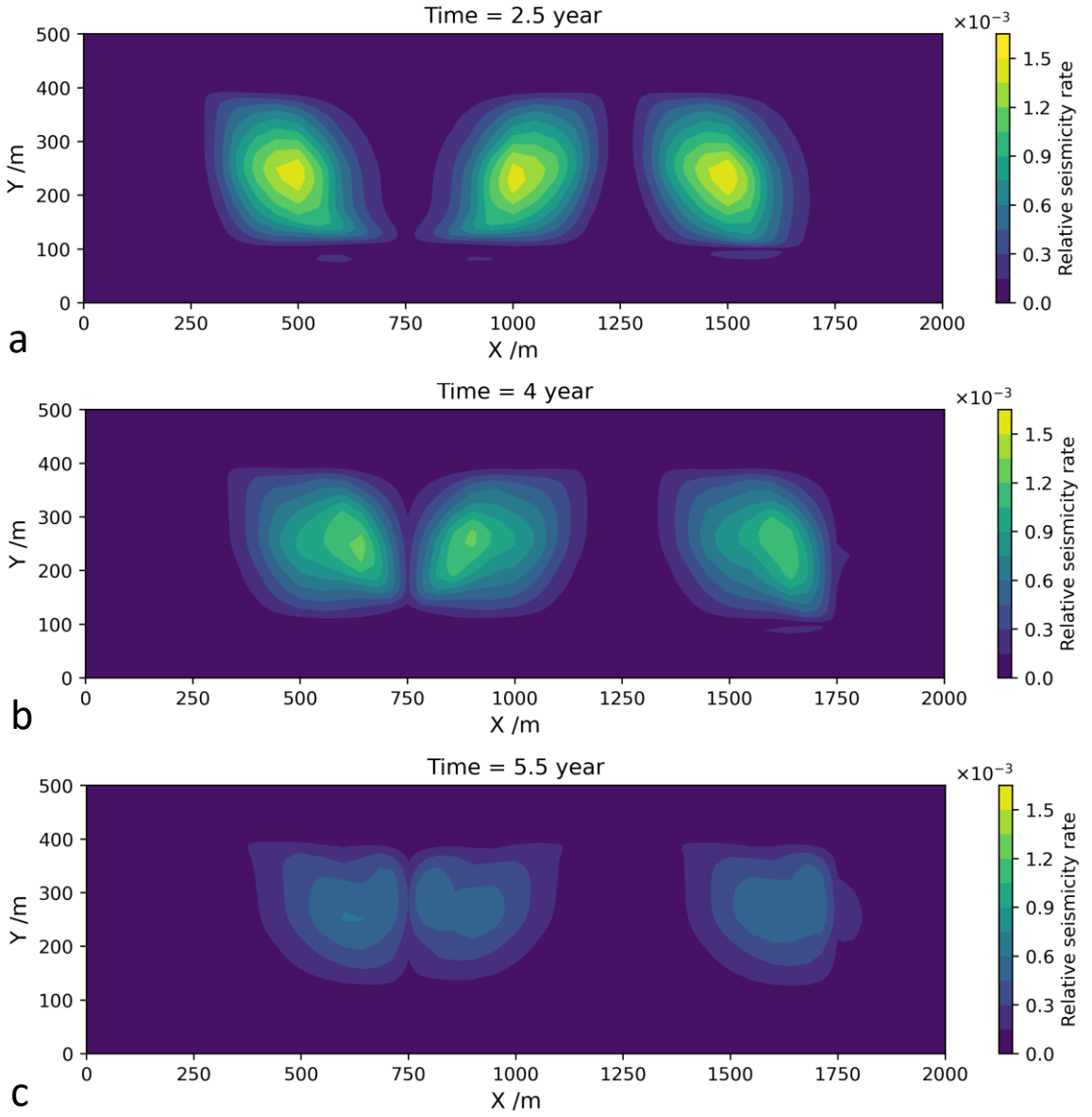

Figure 10: Relative distribution in seismicity rate for the permeability enhancement model at different times during thermal breakthrough (a: t = 2.5 year; b: t = 4.5 year; c: t = 5.5 year) on a horizontal plane cutting the reservoir at z = -3000m.

4. CONCLUSION

We use numerical models to investigate permeability enhancement and induced seismicity during a 20-year production period in an EGS reservoir penetrated by four partially bridging fractures spanning a doublet horizontal well design. A 3D THM reservoir-fracture-wellbore coupling model was built using the FEHM simulator. A stress-dependent permeability model considering the thermo-poroelastic effect was used to simulate permeability evolution during the production period. Induced seismicity was modelled as a function of excess shear stress changes over time. Our main conclusions are summarized as:

(1) During the EGS production period, consideration of permeability enhancement may accelerate thermal breakthrough and increase in injectivity under constant injection pressure conditions – with concomitant increase in power/energy-recovery-rate.

(2) More thermal energy is extracted during the production period, but more seismicity is induced when accommodating SRV permeability enhancement.

(3) Both the permeability enhancement front and seismicity patterns migrate from injection fractures to production fractures as production time increases, and these appear to be associated with the reservoir temperature distribution.

(4) Most seismic events are generated before thermal breakthrough when there is a larger temperature contrast between the injection fractures and the reservoir.

Future work of this research could include optimizing the number and length fractures for the proposed partially bridging fracture design to achieve maximum thermal energy extraction while simultaneously delaying thermal breakthrough and reducing induced seismicity rates. Follow up work could also analyze relative contributions by thermoelastic and poroelastic effects on permeability enhancement and seismicity rate.

ACKNOWLEDGEMENTS

The authors would like to acknowledge the support from the NZ MBIE Endeavour "Empowering Geothermal" research program and US Department of Energy Grant DE-EE0008763.

REFERENCES

Chamorro, C. R., García-Cuesta, J. L., Mondéjar, M. E., & Pérez-Madrazo, A. (2014). Enhanced geothermal systems in Europe: An estimation and comparison of the technical and sustainable potentials. *Energy*, *65*, 250–263.

Dempsey, D., Kelkar, S., Davatzes, N., Hickman, S., & Moos, D. (2015). Numerical modeling of injection, stress and permeability enhancement during shear stimulation at the Desert Peak Enhanced Geothermal System. *International Journal of Rock Mechanics and Mining Sciences*, *78*, 190-206.

Gringarten, A. C., Witherspoon, P. A., & Ohnishi, Y. (1975). Theory of heat extraction from fractured hot dry rock. *Journal of Geophysical Research*, *80*(8), 1120–1124.

Han, S., Cheng, Y., Gao, Q., Yan, C., & Zhang, J. (2019). Numerical study on heat extraction performance of multistage fracturing Enhanced Geothermal System. *Renewable Energy*, *149*, 1214-1226.

Jaeger, J. C., Cook, N. G., & Zimmerman, R. (2009). *Fundamentals of rock mechanics*. John Wiley & Sons.

Jung, R. (2013). EGS — Goodbye or Back to the Future. *Paper presented at the ISRM International Conference for Effective and Sustainable Hydraulic Fracturing*, Brisbane, Australia.

Kelkar, S., Lewis, K., Karra, S., Zyvoloski, G., Rapaka, S., Viswanathan, H., ... & Pawar, R. (2014). A simulator for modeling coupled thermo-hydro-mechanical processes in subsurface geological media. *International Journal of Rock Mechanics and Mining Sciences*, *70*, 569-580.

Lee, H. S., & Cho, T. F. (2002). Hydraulic characteristics of rough fractures in linear flow under normal and shear load. *Rock mechanics and rock engineering*, *35*(4), 299-318.

Lei, Z., Zhang, Y., Zhang, S., Fu, L., Hu, Z., Yu, Z., Li, L., & Zhou, J. (2020). Electricity generation from a three-horizontal-well enhanced geothermal system in the Qiabuqia geothermal field, China: Slickwater fracturing treatments for different reservoir scenarios. *Renewable Energy*, *145*, 65–83.

Riffault, J., Dempsey, D., Karra, S., & Archer, R. (2018). Microseismicity cloud can be substantially larger than the associated stimulated fracture volume: the case of the Paralana Enhanced Geothermal System. *Journal of Geophysical Research: Solid Earth*, *123*(8), 6845-6870.

Riffault, J. (2019). *Understanding the Relationship between Hydraulic Properties of Rocks and Induced Seismicity in the Stimulation of Enhanced Geothermal Systems* (Doctoral dissertation, ResearchSpace@ Auckland).

Shiozawa, S., & Mcclure, M. (2014). EGS Designs with Horizontal Wells, Multiple Stages, and Proppant. *PROCEEDINGS*, Thirty-Ninth Workshop on Geothermal Reservoir Engineering.

Tester, Jefferson W., Anderson, B. J., Batchelor, A. S., Blackwell, D. D., & DiPippo, R. (2006). The Future of Geothermal Energy - Impact of Enhanced Geothermal Systems (EGS) on the United States in the 21st Century. *MIT - Massachusetts Institute of Technology*, *358*.

Townend, J., & Zoback, M. D. (2000). How faulting keeps the crust strong. *Geology*, *28*(5), 399-402.

Xu, T., Yuan, Y., Jia, X., Lei, Y., Li, S., Feng, B., Hou, Z., & Jiang, Z. (2018). Prospects of power generation from an enhanced geothermal system by water circulation through two horizontal wells: A case study in the Gonghe Basin, Qinghai Province, China. *Energy*, *148*, 196–207.

Yu, P., Dempsey, D., & Archer, R. (2021). A three-dimensional coupled thermo-hydro-mechanical numerical model with partially bridging multi-stage contact fractures in horizontal-well enhanced geothermal system. *International Journal of Rock Mechanics and Mining Sciences*, *143*, 104787.

Yu, P., Dempsey, D., & Archer, R. (2022). Techno-Economic feasibility of enhanced geothermal systems (EGS) with partially bridging Multi-Stage fractures for district heating applications. *Energy Conversion and Management*, *257*, 115405.

Zyvoloski, G. A., Robinson, B. A., Dash, Z. V., & Trease, L. L. (1997). *Summary of the models and methods for the FEHM application-a finite-element heat-and mass-transfer code* (No. LA-13307-MS). Los Alamos National Lab. (LANL), Los Alamos, NM (United States).